

## Invited Research Article

# Sources and transport of plutonium in the Indo-Pacific Intersection: Implications for South China Sea freshwater transport into Indonesian Seas

Tengxiang Xie<sup>a</sup>, Minhan Dai<sup>a,\*</sup>, Faisal Hamzah<sup>a,b</sup>, Zhimian Cao<sup>a</sup>, Xianghui Guo<sup>a</sup><sup>a</sup> State Key Laboratory of Marine Environmental Science & College of Ocean and Earth Sciences, Xiamen University, Xiamen, China<sup>b</sup> Institute for Marine Research and Observation, Ministry of Marine Affairs and Fisheries, Bali, Indonesia

## ARTICLE INFO

Editor: Dr. Hailiang Dong

## Keywords:

Indo-Pacific Intersection  
Plutonium isotopes  
Sources  
Transport  
South China Sea  
Freshwater

## ABSTRACT

The Indo-Pacific Intersection (IPI), centered in the Indonesian Seas (IS) and South China Sea (SCS), is a convergence zone of both hydrological and atmospheric circulations and plays an important role in the water cycle and global climatic system. This study presents a unique dataset of both  $^{239+240}\text{Pu}$  activities and  $^{240}\text{Pu}/^{239}\text{Pu}$  atom ratios to trace Plutonium (Pu) source terms and their transport in the IPI, to examine constituent water masses, notably freshwater fluxes. The  $^{240}\text{Pu}/^{239}\text{Pu}$  atom ratios in surface IPI seawater ranged from 0.194 to 0.258 with an average of  $0.223 \pm 0.021$ , values that were consistently higher than global fallout ( $\sim 0.18$ ).  $^{239+240}\text{Pu}$  activities ranged widely from 0.55 to 2.8  $\text{mBq m}^{-3}$  with a generally accumulating trend from the western Pacific Ocean (WP) to the IPI as previously observed. We further reveal, using a two end-member mixing model between global fallout and Pacific Proving Grounds (PPG), that the PPG source contributes  $34 \pm 8\%$  of the Pu to the IS. In the IS, both  $^{239+240}\text{Pu}$  activities and  $^{240}\text{Pu}/^{239}\text{Pu}$  atom ratios further show values between those in the WP and SCS, indicating a two-endmember mixing scheme between the SCS (characteristically lower-salinity but higher PPG Pu-fraction) and the WP (higher-salinity and higher PPG Pu-fraction). We estimate the fractional contribution of the SCS water mass as  $35 \pm 16\%$  in the surface mixed layer and  $49 \pm 14\%$  in the IS 50–235 m depth interval. This water mass transport is equivalent to a freshwater influx of  $80 \pm 47 \text{ mSv}$  from the SCS to the IS (known as the South China Sea Throughflow (SCSTF), a branch of the Indonesian Throughflow (ITF)). It accounts for over half ( $53 \pm 31\%$ ) of the total freshwater flux transported by the ITF into the Indian Ocean and supplies  $\sim 24\%$  the freshwater net evaporation in the Indian Ocean over the  $8^\circ\text{N} - 32^\circ\text{S}$  latitudinal range, and it is thus crucial in maintaining the fresh water balance therein. This freshwater influx to the IS from the SCS also leads to a  $\sim 0.2 \text{ kg m}^{-3}$  decrease in the mean density of the upper 235 m water layer, which serves to inhibit the transport of upper layer warm water from the western tropical Pacific warm pool into the Indian Ocean. Therefore, the SCS, together with the SCSTF, play a critical role in regulating freshwater and heat balance in the IPI and Indian Ocean. These findings have strong implications for the integrative role of the SCS and SCSTF on the Indo-Pacific climate and water cycle.

## 1. Introduction

The Indo-Pacific Intersection (IPI), primarily including the Indonesian Seas (IS) and South China Sea (SCS), is where the tropical western Pacific Ocean (WP) and the eastern Indian Ocean intersect (Fig. 1). As a convergence zone of both hydrological and atmospheric circulations, the IPI is an important component of the global hydrological cycle (Yamanaka et al., 2018). The IS, connecting the WP and Indian Oceans, is also a key route for global ocean circulation. The large amount of water mass transfer between the Pacific and Indian Oceans through the IS is commonly referred to as the Indonesian Throughflow (ITF), and is important in

regulating the freshwater inventories of the Indian Ocean and the global hydrological cycle (Gordon, 1986; Gordon, 2005; Sprintall et al., 2014).

The SCS, the largest marginal sea of the North Pacific Ocean, receives a large flow of freshwater ( $\sim 0.112 \text{ Sv}$ ) from land discharge and from precipitation minus evaporation ( $P - E$ ) (Fang et al., 2009). This buoyant freshwater concentrates in the upper layer of the SCS and spreads into adjacent seas/oceans. The SCS branch of the Pacific-Indian Ocean Throughflow (SCSTF) is an important contributor to the ITF that largely influences the sea surface temperature (SST) and salinity within the Indonesian Maritime Continent (IMC) (e.g., Gordon et al., 2003; Qu et al., 2006), and the ITF's main flow and variability (e.g., Li et al.,

\* Corresponding author.

E-mail address: [mdai@xmu.edu.cn](mailto:mdai@xmu.edu.cn) (M. Dai).<https://doi.org/10.1016/j.chemgeo.2021.120367>

Received 22 March 2021; Received in revised form 26 May 2021; Accepted 31 May 2021

Available online 1 June 2021

0009-2541/© 2021 The Authors.

Published by Elsevier B.V. This is an open access article under the CC BY-NC-ND license

<http://creativecommons.org/licenses/by-nc-nd/4.0/>.

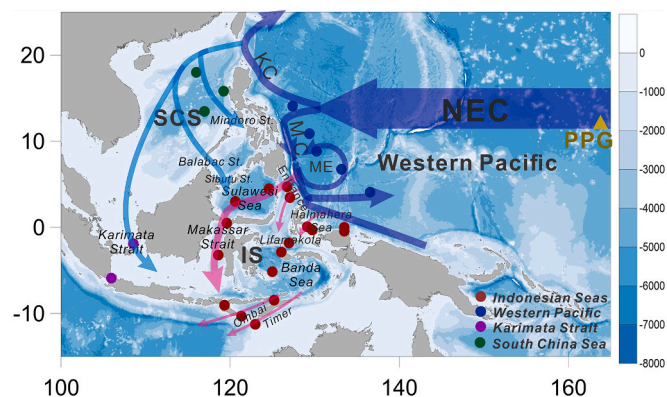


**Fig. 1.** Map of the Indo-Pacific Intersection showing locations of the sampling stations, and main oceanic currents in the region. Red, blue, pink and green circles indicate the stations sampled in the Indonesian Seas, the Western Pacific Ocean, Karimata Strait and South China Sea (SCS), respectively. PPG indicates the Pacific Proving Grounds; ME, NEC, KC and MC denote the Mindoro eddy, North Equatorial, Kuroshio and Mindoro currents, respectively. (For interpretation of the references to colour in this figure legend, the reader is referred to the web version of this article.)

2019). Given that nutrient levels in the upper SCS are higher than in the western IS and WP (Gutknecht et al., 2016), the SCSTF is also a potential nutrient source sustaining the IMC ecosystem. Long-term observations conducted during 2008–2015 revealed the SCSTF transport of 1.99 Sv through the Karimata Strait during boreal winter, but this flow reverses during boreal summer, with a seasonal variability of 2.68 Sv (Wang et al., 2019). Different numerical models also yielded a large range, from 0.3 to 1.6 Sv, in the annual-mean-volume transport through the Karimata Strait (Fang et al., 2009; Gan et al., 2016; Guohong et al., 2005; He et al., 2015; Tozuka et al., 2009; Yaremchuk et al., 2009). The Mindoro Straits and Sibutu Passage provide secondary SCS branch portals that allow water to enter the IS. Numerical models reveal a  $3.2 \pm 1.2$  Sv transport out from the SCS through the Mindoro Straits (Gan et al., 2016). However, three simultaneous moored time-series in Mindoro, Tablas and Panay Straits showed that the mean annual transport from the SCS into the Sulu Sea during 2008 was almost null (0.1 Sv) (Sprintall et al., 2012). The large range of the estimated flux might be due to the high seasonal and inter-annual variability of the SCSTF in responding to the Asian monsoon and/or the El Niño-Southern Oscillation (ENSO), recognized as the largest source of uncertainty of the Pacific-Indian Oceans throughflow pathways (Gordon et al., 2003; He et al., 2015). Such knowledge gaps largely restrict our understanding of the freshwater transport from the SCS to the IS and the role of the SCS and its throughflow on the regional hydrological cycle. It thus becomes crucially important to better constrain the transport of the SCS water mass into the IS.

Plutonium (Pu) is a man-made element released from above-ground nuclear weapons testing, and accidental releases and discharges from reprocessing plants (Dai et al., 2005; Kershaw et al., 1995; Sholkovitz, 1983; Zheng et al., 2012). It is released into the marine environment and transported far from the point source by ocean currents. One of the most important sources of Pu in the northern Pacific is the Pacific Proving Grounds (PPG) in the Marshall Islands, located in the vicinity of the North Equatorial Current (NEC), that released >50% of the total fallout input during 1952–1958 and 20% of the global fallout by the end of atmospheric testing (Buesseler, 1997; Buesseler et al., 2018). Whereas the average global fallout  $^{240}\text{Pu}/^{239}\text{Pu}$  atom ratio is  $0.178 \pm 0.019$  (0–30°N) (Kelley et al., 1999; Krey et al., 1975), close-in fallout traceable to the PPG has a very high  $^{240}\text{Pu}/^{239}\text{Pu}$  atom ratio of  $0.33 \pm 0.03$  (Buesseler, 1997; Muramatsu et al., 2001). The Pu isotopic composition with characteristically high ratios in sediments of the northern SCS and IS revealed that Pu was continuously released and transported into the

IPI from the PPG (Pittauer et al., 2017; Wu et al., 2014). Due to the different water sources and Pu accumulation time in the SCS, IS and WP, these will differ in their Pu activities and isotopic compositions, thus providing fingerprints to help our understanding of water mass transport in the IPI.

This study presents the distribution of Pu activity and isotopic composition in the IPI with an aim to determine the sources and transport pathways of Pu. The Pu signals in different water masses allow tracing of some of the Pacific-Indian Ocean throughflow waters back to their sources in the IPI, which in turn are used to quantify water mass and freshwater transport in the IPI and thus improve our understanding of the regional and global hydrological cycle.

## 2. Materials and methods

### 2.1. Study area

The IS and SCS are the two main regions in the IPI. The former, located between the Pacific and Indian Oceans, connects the two eastern and western warm pools. Thousands of islands within this IMC generate interlaced pathways for Pacific-Indian Ocean throughflow (Fig. 1). The primary inflow passage of the ITF is provided by the Makassar Strait with waters largely drawn from the energetic Mindanao retroflection (Sprintall et al., 2014). Additionally, the shallower waters from the South Pacific are found entering through the Halmahera Sea. The water in the IS exits into the Indian Ocean through the Lombok and Ombai Straits, and the Timor Passage. The SCS has a semi-enclosed deep basin and exchanges water with the WP through the Luzon Strait. A branch of the Kuroshio Current intrudes from the WP into the SCS upper layer (~400 m deep) and modulates the surface seawater chemistry of the northern SCS (Du et al., 2013; Wu et al., 2018). After being modified by physical and biogeochemical processes, most of the SCS water mass exits into the IS through the Karimata and Mindoro/Balabac Straits, and then joins the ITF to flow into the Indian Ocean.

### 2.2. Sample collection and data

Samples in the IS were collected during a September to November 2017 cruise onboard R/V Baruna Jaya VIII, which covered both the primary (Sulawesi Sea to Makassar Strait) and eastern (Lifamatola to Banda Sea) pathways of the ITF (Fig. 1). The entrance and exit of the ITF were also sampled. Samples in the Karimata Strait were collected in June 2015. Sampling in the WP, located at the gateway of the IS water source, was conducted onboard the R/V Dongfanghong II in December 2015. Pu data in the SCS were collected in April 2012 (Wu et al., 2018). Samples in the Karimata Strait were collected using Niskin bottles on a conductivity, temperature, depth (CTD) rosette system in the surface and at ~45 m depth, and all other samples were collected from the surface using a pumping system. Upon collection, seawater samples (~100 L in volume) were acidified with concentrated  $\text{HNO}_3$  to a  $\text{pH}$  of  $1.6 \pm 0.1$  to destroy hydrolysis products or complexes of Pu so as to favor formation of oxidized Pu (V-VI) for subsequent sample processing and Pu isotope measurements (Choppin, 2006; Wu et al., 2018).

### 2.3. Sample processing and Pu isotope analysis

The Pu analytical method used in seawater has been described elsewhere (Buesseler and Halverson, 1987; Wu et al., 2018; Zheng and Yamada, 2007). Briefly, a known amount of  $^{242}\text{Pu}$  (Institute for Reference Materials and Measurements (IRMM)-085, European Commission Joint Research Centre, Belgium) was added to the seawater samples as a yield determinant. Plutonium in the spiked sample was coprecipitated with ferric hydroxide by adding ~10 mL of an  $\text{Fe}^{3+}$  solution ( $15.5 \text{ mg mL}^{-1}$ ) and adjusting the pH to ~9 with the addition of concentrated  $\text{NH}_4\text{OH}$ . The precipitate was then dissolved in 40 mL of 8 M  $\text{HNO}_3$ , and then  $\text{NaNO}_2$  was added to adjust the Pu valence state to  $\text{Pu}^{4+}$ . Plutonium

in the solution was subsequently purified with two stage anion-exchange columns using AG 1-X8 and AG MP-1 M (Bio-Rad) (Bu et al., 2014c; Wu et al., 2018; Zheng and Yamada, 2007). The final solution, evaporated to near dryness, was dissolved in 4% ultrapure HNO<sub>3</sub> (1.0 mL) and analyzed using a Multicollector-Inductively Coupled Plasma Mass Spectrometer (MC-ICP-MS) (Nu Plasma HR, Nu Instruments Ltd., England) in the State Key Laboratory of Marine Environmental Science, Xiamen University. The Aridus3 high-efficiency sample introduction system with a membrane desolvation unit and a conical concentric nebulizer was used. Plutonium recovery resulting from this procedure was  $65.2 \pm 10.7\%$  ( $n = 25$ ). In addition, the formation of polyatomic uranium hydrides ( $^{238}\text{UH}^+$ ) and peak tailing from the  $^{238}\text{U}^+$  peak are the most significant interference in this method, resulting in overestimation of the  $^{239}\text{Pu}$  signal. The analytical method employed in this study effectively eliminated U interferences by achieving an extremely high U decontamination factor of  $3\text{--}7 \times 10^7$ , which is comparable to previously reported values ( $3.0 \times 10^7\text{--}1.0 \times 10^8$ ) (Bu et al., 2014b; Wu et al., 2018).

Data quality and mass bias correction were assured by routine analysis of International Atomic Energy Agency (IAEA) certified reference material IAEA-443 (Irish Seawater). The measured  $^{239+240}\text{Pu}$  activities and  $^{240}\text{Pu}/^{239}\text{Pu}$  atom ratios of this standard (activity:  $14.8 \pm 0.3$  mBq kg<sup>-1</sup>; ratio:  $0.230 \pm 0.004$ ,  $n = 23$ ) were consistent with the verified value (activity:  $14.7 \pm 0.3$  mBq kg<sup>-1</sup>; ratio:  $0.229 \pm 0.006$ ) (Pham et al., 2011). In addition, the operational blank count rates for  $^{239}\text{Pu}$  and  $^{240}\text{Pu}$  were assessed by measuring 100 L of pure water following the same chemical procedure was used for Pu determination in seawater. The limit of detection (LOD) was calculated based on International Union of Pure and Applied Chemistry recommendations (Mocak et al., 1997); it was estimated at 0.01 and 0.03 mBq m<sup>-3</sup> for  $^{239}\text{Pu}$  and  $^{240}\text{Pu}$ , respectively.

### 3. Results

#### 3.1. Hydrography

As shown in Fig. 2, surface water samples collected in the WP exhibit a higher salinity (34.28 to 34.73). In contrast, the salinity in SCS-related regions (SCS basin and Karimata Strait) is lower because the SCS receives  $3.54 \times 10^{12}$  m<sup>3</sup> year<sup>-1</sup> freshwater from land discharge and precipitation - evaporation (P-E) (Fang et al., 2009). The fresher SCS water mass thus exhibits a lower density than the IS and WP water masses. The salinity in the IS falls in between that in SCS-related regions and WP, ranging from 33.59 to 34.02. Due to the non-conservative behavior of temperature related to the solar radiation in the surface layer, the obviously spatial temperature pattern of different regions is not observed. However, the temperature between 5°N and 5°S is visibly higher than that south of 5°S in the IS.

#### 3.2. Spatial distribution of Pu in the Indo-Pacific Intersection

##### 3.2.1. $^{240}\text{Pu}/^{239}\text{Pu}$ atom ratios

As shown in Table 1,  $^{240}\text{Pu}/^{239}\text{Pu}$  atom ratios of surface seawater in the IPI varied from 0.194 to 0.258, with an average of  $0.223 \pm 0.021$  ( $n = 28$ , number of samples, NO.1–28), which is comparable to previously reported values in the WP and its marginal seas ( $0.227 \pm 0.018$ ,  $n = 11$ , obtained in 1996; Yamada et al., 2006).

$^{240}\text{Pu}/^{239}\text{Pu}$  atom ratios in the IPI show notable spatial variation (Fig. 3). In the WP surface water, even lower  $^{240}\text{Pu}/^{239}\text{Pu}$  atom ratios than those in the SCS and IS are observed, with an average of  $0.200 \pm 0.005$  ( $n = 5$ ). The comparison of  $^{240}\text{Pu}/^{239}\text{Pu}$  atom ratio at station WP6 ( $0.194 \pm 0.006$ ) with that in the previous observation at a similar location (PAS04:  $0.201 \pm 0.035$ ;  $14.54^\circ\text{N}/128.22^\circ\text{E}$ ; Yamada et al., 2006) and that at a sample outside Guam also collected in 2015 ( $0.198 \pm 0.016$ , 100 m;  $16.00^\circ\text{N}/156.83^\circ\text{E}$ ; Buesseler et al., 2018), indicates that they are very consistent.

$^{240}\text{Pu}/^{239}\text{Pu}$  atom ratios in the SCS basin ( $0.244 \pm 0.004$ ,  $n = 3$ ) generally

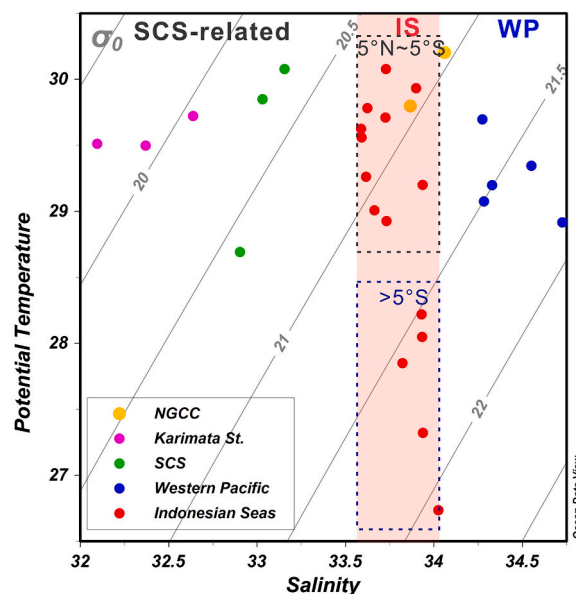


Fig. 2. Salinity vs. temperature (°C) diagram of the surface waters. Red, blue, pink, green and orange circles indicate samples collected in the Indonesian Seas (IS), Western Pacific Ocean (WP), Karimata Strait, South China Sea (SCS), and New Guinea coastal current (NGCC), respectively. The samples collected in the IS are shaded. The black and blue dashed boxes indicate the samples between 5°N and 5°S and south of 5°S, respectively. (For interpretation of the references to colour in this figure legend, the reader is referred to the web version of this article.)

exhibit higher values than those in the IPI (Wu et al., 2018). The highest  $^{240}\text{Pu}/^{239}\text{Pu}$  ratios of  $0.257 \pm 0.001$  ( $n = 2$ ) measured in the Karimata Strait may be related to the dynamic exchange at the sediment-water interface in this shallow strait (depth: ~45 m). Indeed, the  $^{240}\text{Pu}/^{239}\text{Pu}$  ratio in sediment exhibits a higher value than that in the overlying water column at a similar location (Wu et al., 2014, 2018). Strong tidal mixing would likely result in release of Pu with high ratios from sediment. The vertical profile in the Karimata Strait featuring higher  $^{240}\text{Pu}/^{239}\text{Pu}$  ratios ( $0.269 \pm 0.007$ ) in bottom than in surface water supports this view (Table 1, B3 station).

$^{240}\text{Pu}/^{239}\text{Pu}$  ratios in the IS are intermediate between these in the WP and SCS, with an average of  $0.223 \pm 0.011$  ( $n = 15$ ). The lowest  $^{240}\text{Pu}/^{239}\text{Pu}$  ratios are observed at the ITF entrance due to the input of the WP water mass ( $0.213 \pm 0.03$ ,  $n = 4$ ). Along the main trajectory of the ITF, the  $^{240}\text{Pu}/^{239}\text{Pu}$  ratios increase south of the Sulawesi Sea (IND-101) and Makassar Strait (IND103–107) with a mean value of  $0.225 \pm 0.006$  ( $n = 3$ ). The  $^{240}\text{Pu}/^{239}\text{Pu}$  ratio obtained at the entrance of the Makassar Strait ( $0.231 \pm 0.004$ ) is similar to the previous observation at the same location ( $0.234 \pm 0.026$ ) (Yamada et al., 2006). The SCS water mass with high  $^{240}\text{Pu}/^{239}\text{Pu}$  ratios transported from the Sibutu Strait moves southwardly and adds to the ITF in the north of the Makassar strait, as a “checkpoint”, resulting in increases in the  $^{240}\text{Pu}/^{239}\text{Pu}$  ratios. Due to the water mass mixing and riverine input, the SCS water mass signal decreases along the ITF pathway and exhibit lower  $^{240}\text{Pu}/^{239}\text{Pu}$  ratios in the south of the Makassar strait. In the eastern IS (Lifamatola Strait and Banda Sea) and the ITF exit trajectory,  $^{240}\text{Pu}/^{239}\text{Pu}$  ratios are also higher than those at the ITF entrance, with values of  $0.224 \pm 0.004$  ( $n = 3$ ) and  $0.238 \pm 0.004$  ( $n = 3$ ), respectively. At the exit of the IS, the buoyancy SCS water passing through Karimata Strait (SCSTF) carries water masses with higher  $^{240}\text{Pu}/^{239}\text{Pu}$  ratios into the Sunda, Savu and Sumba Straits and join the ITF.

##### 3.2.2. $^{239+240}\text{Pu}$ activities

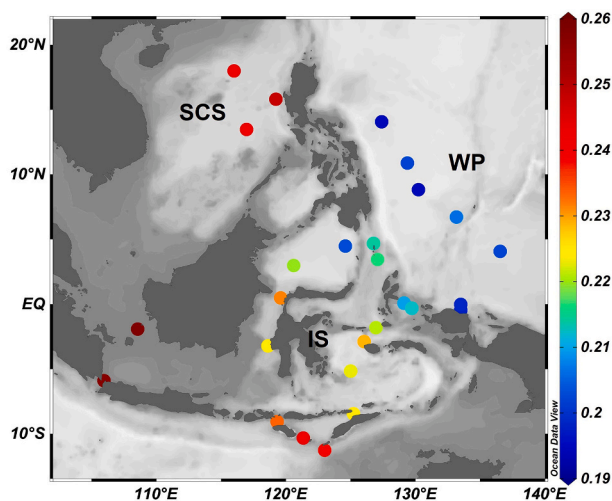
$^{239+240}\text{Pu}$  activities in IPI surface seawater are also listed in Table 1. They varied from 0.55 to 0.28 mBq m<sup>-3</sup>, averaging  $1.68 \pm 0.67$  mBq

**Table 1**Mean  $^{239+240}\text{Pu}$  activities and  $^{240}\text{Pu}/^{239}\text{Pu}$  atom ratios in surface seawater of the Indo-Pacific Intersection at different stations (latitudes and longitudes indicated).

NO.	Area	Station	Lat.	Long.	Date	Layer (m)	T	S	$^{239+240}\text{Pu}$ ( $\text{mBq m}^{-3}$ )	$^{240}\text{Pu}/^{239}\text{Pu}$
1	IS	IND-4	119.32	-9.05	2017/9/19	1	26.74	34.02	$2.80 \pm 0.07$	$0.233 \pm 0.005$
2		IND-7	121.35	-10.31	2017/9/21	1	27.32	33.94	$2.10 \pm 0.05$	$0.241 \pm 0.008$
3		IND-13	122.98	-11.25	2017/9/22	1	28.05	33.93	$1.68 \pm 0.06$	$0.238 \pm 0.009$
4		IND-17	125.21	-8.44	2017/9/25	1	28.22	33.93	$2.22 \pm 0.06$	$0.224 \pm 0.008$
5		IND-29	124.99	-5.15	2017/9/27	1	27.85	33.82	$1.59 \pm 0.05$	$0.223 \pm 0.009$
6		IND-35	126.04	-2.87	2017/9/28	1	28.93	33.73	$1.33 \pm 0.04$	$0.229 \pm 0.014$
7		IND-44	126.95	-1.80	2017/10/8	1	29.01	33.66	$1.95 \pm 0.05$	$0.221 \pm 0.007$
8		IND-64	129.11	0.08	2017/10/10	1	29.93	33.90	$0.57 \pm 0.02$	$0.210 \pm 0.010$
9		IND-66	129.70	-0.31	2017/10/12	1	29.20	33.94	$0.71 \pm 0.03$	$0.212 \pm 0.008$
10		IND-84	127.07	3.46	2017/11/1	1	30.08	33.73	$1.23 \pm 0.05$	$0.216 \pm 0.014$
11		IND-86	126.76	4.70	2017/11/3	1	29.56	33.59	$1.13 \pm 0.04$	$0.214 \pm 0.012$
12		IND-92	124.59	4.50	2017/11/4	1	29.71	33.73	$1.19 \pm 0.03$	$0.203 \pm 0.010$
13		IND-101	120.60	3.00	2017/11/7	1	29.63	33.59	$1.65 \pm 0.05$	$0.220 \pm 0.011$
14		IND-103	119.60	0.50	2017/11/8	1	29.26	33.62	$2.42 \pm 0.04$	$0.231 \pm 0.004$
15		IND-107	118.61	3.21	2017/11/10	1	29.78	33.62	$2.00 \pm 0.06$	$0.224 \pm 0.010$
16	WP	IND-68	133.49	-0.44	2017/10/13	1	29.80	33.87	$0.55 \pm 0.02$	$0.198 \pm 0.009$
17		IND-69	133.50	0.00	2017/10/13	1	30.20	34.06	$0.57 \pm 0.02$	$0.198 \pm 0.015$
18		WP6	127.39	14.08	2015/12/11	1	28.92	34.73	$1.54 \pm 0.04$	$0.194 \pm 0.006$
19		WP7	129.38	10.89	2015/12/12	1	29.08	34.28	$1.55 \pm 0.04$	$0.202 \pm 0.010$
20		WP8	130.22	8.84	2015/12/13	1	29.20	34.33	$1.21 \pm 0.03$	$0.194 \pm 0.011$
21		WP9	133.15	6.74	2015/12/14	1	29.70	34.27	$1.27 \pm 0.04$	$0.206 \pm 0.008$
22		WP10	136.55	4.09	2015/12/15	1	29.35	34.55	$1.60 \pm 0.06$	$0.202 \pm 0.012$
23	KS	East	105.95	-5.88	2015/6/9	1	29.72	32.64	$2.10 \pm 0.05$	$0.257 \pm 0.007$
24		B3	108.54	-1.91	2015/6/13	1	29.50	32.37	$2.54 \pm 0.05$	$0.258 \pm 0.004$
25		B3	108.54	-1.91	2015/6/13	39	29.52	32.09	$2.24 \pm 0.04$	$0.269 \pm 0.007$
26	SCS	SEATS	116.00	18.00	2012/8/6	1	28.69	32.90	$2.35 \pm 0.04$	$0.242 \pm 0.007$
27		M1	119.23	15.80	2012/4/16	1	29.85	33.03	$2.78 \pm 0.04$	$0.248 \pm 0.004$
28		O7	116.96	13.47	2012/4/22	1	30.08	33.16	$2.42 \pm 0.05$	$0.241 \pm 0.006$

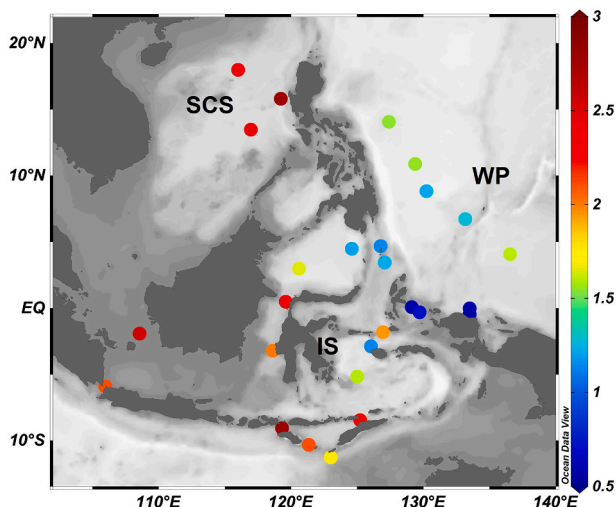
T: temperature; S: salinity.

IS: Indonesian Seas; WP: Western Pacific Ocean; KS: Karimata Strait; SCS: South China Sea (Wu et al., 2018).

**Fig. 3.** Surface distribution of  $^{240}\text{Pu}/^{239}\text{Pu}$  atom ratios in the Indo-Pacific Intersection. IS, WP and SCS denote the Indonesian Seas, Western Pacific Ocean and South China Sea, respectively.

$\text{m}^{-3}$  ( $n = 28$ , No.1–28). These  $^{239+240}\text{Pu}$  activity levels are lower than those previously reported in the WP and its marginal seas ( $2.43 \pm 0.71 \text{ mBq m}^{-3}$ ,  $n = 11$ , collected in 1996), implying that Pu is spreading with oceanic currents and is being scavenged from surface IPI water (Yamada et al., 2006).

Spatial variation of  $^{239+240}\text{Pu}$  activities in the IPI is shown in Fig. 4. The WP  $^{239+240}\text{Pu}$  activities ( $1.43 \pm 0.18 \text{ mBq m}^{-3}$ ,  $n = 5$ ) are lower than those in its marginal seas ( $1.72 \pm 0.73 \text{ mBq m}^{-3}$ ,  $n = 22$ ), suggesting significant Pu accumulation within marginal seas as previously reported in the SCS (Wu et al., 2018). Since the residence time of the water mass in the SCS (~40 years) is longer than that in the IS (5.6 years), the SCS accumulates more Pu (Liu and Gan, 2017; Xie et al.,

**Fig. 4.** Surface distribution of  $^{239+240}\text{Pu}$  activities in the Indo-Pacific Intersection. IS, WP and SCS denote the Indonesian Seas, Western Pacific Ocean and South China Sea, respectively.

2019). Additionally, the IS water masses are drawn from both the high-energy Mindanao (mainly North Pacific water) and Halmahera (mainly South Pacific) retroreflections, accounting for 10–30% of the inflow of the ITF from the South Pacific Ocean (Morey et al., 1999; Sprintall et al., 2014). Because most atmospheric nuclear weapons tests were conducted in the North Pacific,  $^{239+240}\text{Pu}$  activities in the South Pacific Ocean exhibit lower values (Hirose et al., 2007), as also supported by the low values obtained at stations in the Papua New Guinea Coastal Current ( $0.56 \pm 0.01 \text{ mBq m}^{-3}$ ,  $n = 2$ ). Thus, due to the different Pu sources and magnitude of accumulation in the IPI, the SCS ( $2.52 \pm 0.23 \text{ mBq m}^{-3}$ ,  $n = 3$ ) exhibits higher  $^{239+240}\text{Pu}$  activities than those in the IS ( $1.63 \pm 0.64 \text{ mBq m}^{-3}$ ,  $n = 15$ ).

$^{239+240}\text{Pu}$  activities at the ITF entrance are lower than that within the IS as a result of the exchange with WP water mass with lower  $^{239+240}\text{Pu}$  activities (Fig. 4). Furthermore,  $^{239+240}\text{Pu}$  activities at the north entrance ( $1.18 \pm 0.07 \text{ mBq m}^{-3}$ ,  $n = 2$ ) are obviously higher than that those at the south entrance ( $0.64 \pm 0.10 \text{ mBq m}^{-3}$ ,  $n = 2$ ), implying that the surface water at the Halmahera Sea is mainly transported from the South Pacific Ocean. In agreement with the distribution of  $^{240}\text{Pu}/^{239}\text{Pu}$  atom ratios in the IPI, the  $^{239+240}\text{Pu}$  activities increase along the main ITF trajectory from the south of the Sulawesi Sea ( $1.65 \pm 0.05 \text{ mBq m}^{-3}$ ,  $n = 2$ ) to the Makassar Strait ( $2.21 \pm 0.30 \text{ mBq m}^{-3}$ ,  $n = 2$ ), suggesting that additional water sources with high  $^{239+240}\text{Pu}$  activities are transported into the Sulawesi Sea and Makassar Strait. The  $^{239+240}\text{Pu}$  activities at the ITF exit ( $2.19 \pm 0.57 \text{ mBq m}^{-3}$ ,  $n = 3$ ) are also characterized by higher values than those at the ITF entrance.

## 4. Discussion

### 4.1. Plutonium sources and transport

Plutonium originating from different sources has specific characteristics, and  $^{240}\text{Pu}/^{239}\text{Pu}$  atom ratios allow identification of these sources. The  $^{240}\text{Pu}/^{239}\text{Pu}$  atom ratios in the IPI are all characteristically higher than those expected global fallout in the latitude band of IS's water sources ( $0.178 \pm 0.019$ ,  $0\text{--}30^\circ\text{N}$ ) (Kelley et al., 1999), implying that this area must have received Pu from the detonation of high-yield thermonuclear devices and/or high burnup fuel reactors such as the PPG and/or Fukushima Dai-ichi Nuclear Power Plant (FDNPP) accident. Plutonium isotope activities ( $^{239+240}\text{Pu}$  and  $^{241}\text{Pu}$ ) and atom ratios ( $^{240}\text{Pu}/^{239}\text{Pu}$  and  $^{241}\text{Pu}/^{239}\text{Pu}$ ) in seawater and marine sediments within 30 km of the FDNPP site exhibit values that are in the range of background values after the accident, which suggests that released Pu from the FDNPP accident to the marine environment was negligible (Bu et al., 2014a, 2014b). The Bikini and Enewetak Atolls are two representative PPG sites where the USA conducted 66 nuclear weapons tests between 1952 and 1958 (Buesseler, 1997; Buesseler et al., 2018). Based on the residence times in lagoon water derived from radium isotopes, it was estimated that the released  $^{239+240}\text{Pu}$  from the Enewetak and Bikini Atolls into the North Pacific Ocean equaled an annual flux of  $0.26\text{--}0.73 \text{ TBq}$  ( $1 \text{ TBq} = 10^{12} \text{ Bq}$ ) (Buesseler et al., 2018). Because the two atolls are located within the latitudinal NEC band, the released Pu will be transported westward to the western boundary of the WP and intrude into its marginal seas. Thus, the PPG, that continually releases Pu from sediments and groundwater in contaminated lagoons, is another main source term contributing to Pu in the IPI besides global fallout.

Notable variation of  $^{240}\text{Pu}/^{239}\text{Pu}$  ratios was observed in the different regions (SCS, WP and IS) of the IPI (Fig. 3), with the SCS showing the highest  $^{240}\text{Pu}/^{239}\text{Pu}$  ratio. The Kuroshio current, as the main water source for SCS upper water exchange with the WP, is the northward bifurcation of the NEC. It shows an even heavier Pu isotopic ratio than the average value in the WP (Wu et al., 2019). Thus, the SCS receives more Pu generated from the PPG. Inflow waters to the IS are drawn from the Mindanao (mainly North Pacific water) and Halmahera (mainly South Pacific) retroreflections (Sprintall et al., 2014). The  $^{240}\text{Pu}/^{239}\text{Pu}$  ratio in the South Pacific Ocean is lower than that in the Kuroshio current. Although the region of the Mindanao retroreflection receives water from the narrow Mindanao current, which is the southward bifurcation of the NEC, much of the water mass outside the Mindanao current with lower  $^{240}\text{Pu}/^{239}\text{Pu}$  ratios is also mixed into this region by the semi-permanent Mindanao eddy thus serving to dilute the Pu fraction from the PPG. Direct current measurements revealed that the transport of the Mindanao current in the upper 300 m increased from 13 Sv at  $10^\circ\text{N}$  to 33 Sv at  $5.5^\circ\text{N}$  (ITF gateway region) (Lukas et al., 1991). Thus, the WP water source for the IS includes less Pu originating from the PPG than that for the SCS, which results in lower  $^{240}\text{Pu}/^{239}\text{Pu}$  ratios in the IS.

The IS connects both the SCS and WP, and thus variation of the  $^{240}\text{Pu}/^{239}\text{Pu}$  ratios within the IS will be traceable to the water mass

exchange with the SCS and WP. Higher  $^{240}\text{Pu}/^{239}\text{Pu}$  ratios are detected in the southern Sulawesi Sea and Makassar Strait than that at the ITF entrance, which indicates that there is an additional water source transported into these regions with high  $^{240}\text{Pu}/^{239}\text{Pu}$  ratios. Physical modeling and field observations have shown that the SCS water mass is able to exit the SCS through the Mindoro Straits and enter the Sulawesi Sea through the Sibutu Passage (Gan et al., 2016; Gordon et al., 2012; Sprintall et al., 2012). Given the fact that the Sibutu Passage is the main channel transporting SCS water into the IS, and that the  $^{240}\text{Pu}/^{239}\text{Pu}$  in the SCS is higher, the water mass input from the SCS very likely results in the  $^{240}\text{Pu}/^{239}\text{Pu}$  increase in these regions. Since the SCS water mass also exits through the Karimata Strait, the  $^{240}\text{Pu}/^{239}\text{Pu}$  ratios at the ITF exit further increase. The ratios in the eastern IS indeed exhibit higher values than that at entrance, which suggests that the SCS water mass has been transported into this region.

### 4.2. Quantitative estimation of the PPG Pu contribution

The water mass in the IS exhibits quite different  $^{240}\text{Pu}/^{239}\text{Pu}$  atom ratios from those in their source waters in the SCS and WP. The  $^{240}\text{Pu}/^{239}\text{Pu}$  atom ratio in the SCS water endmember ( $0.249 \pm 0.008$ ) is much higher than that in the WP endmember ( $0.199 \pm 0.05$ ). Such difference in  $^{240}\text{Pu}/^{239}\text{Pu}$  atom ratios indicates that the SCS and WP water masses contain different PPG derived Pu-fractions. Thus, the Pu isotopes signal in the IS provide a good tool to trace back the SCS and WP water masses.

The  $^{240}\text{Pu}/^{239}\text{Pu}$  atom ratios determined in the IPI fell well within the characteristic values of global and PPG close-in fallout (Fig. 5). To distinguish the two dominant Pu sources, the relative contribution of the PPG to Pu in the IPI was estimated using a two end-member mixing model (Krey et al., 1975; Wu et al., 2019; Yamada et al., 2006), as follows:

$$\frac{[\text{Pu activity}]_P}{[\text{Pu activity}]_G} = \frac{(R_G - R_w)}{(R_w - R_P)} \frac{(1 + 3.67R_P)}{(1 + 3.67R_G)} \quad (1)$$

where [Pu activity] and  $R$  represent the  $^{239+240}\text{Pu}$  activity and  $^{240}\text{Pu}/^{239}\text{Pu}$  atom ratio; the subscripts  $P$ ,  $G$  and  $W$  refer to the PPG, global fallout and the water samples; and the coefficient 3.674 is a constant used to convert between the  $^{240}\text{Pu}/^{239}\text{Pu}$  activity ratio and atom ratio. In the calculation,  $R_G$  was taken to be  $0.178 \pm 0.019$  (Kelley et al., 1999; Krey et al., 1975) and  $R_P$  was  $0.330 \pm 0.030$  (Buesseler, 1997; Muramatsu et al., 2001).

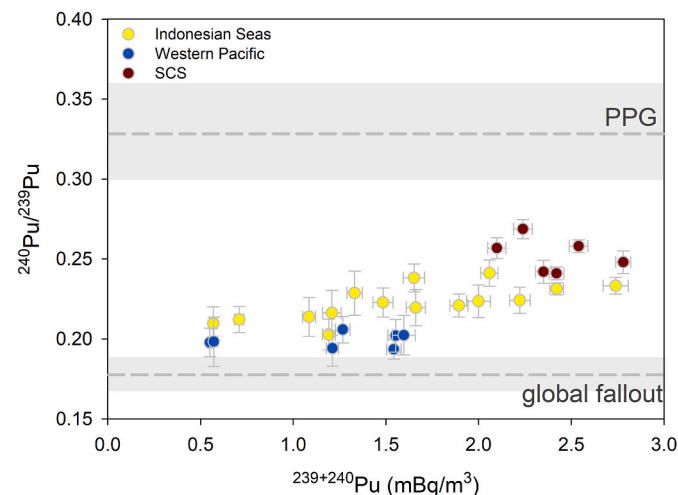


Fig. 5. Relationship between  $^{240}\text{Pu}/^{239}\text{Pu}$  atom ratios and  $^{239+240}\text{Pu}$  activities. Lower and upper dashed lines represent the average atom ratio of the global fallout ( $0.178 \pm 0.019$ ) and that ( $0.33 \pm 0.03$ ) characteristic of the Pacific Proving Grounds (PPG), respectively.

The fractional contribution of Pu derived from PPG in the IPI averaged  $34 \pm 15\%$  ( $n = 28$ ) (Fig. 6), which is somewhat lower than the 1997 estimate made for surface waters of the Southeast Asian Seas ( $\sim 40\%$ ; Yamada et al., 2006). Different sampling coverage between the two studies may be the principal reason for the discrepancy. Alternatively, the Pu fraction from the PPG may have been decreasing over the past 20 years. However, the total flux released from the Bikini and Enewetak sediment and groundwater over the past 60 years is still  $<0.1\%$  of the amount of  $^{239+240}\text{Pu}$  initially delivered via close-in fallout to the North Pacific (Buesseler et al., 2018). The PPG should be considered a stable Pu source during the past 20 years, as is proved by the similar PPG contribution in the northern SCS shelf sediment between 1961 and 1980 and 1981–1999 (Wu et al., 2014). Buesseler (1997) indicated that the close-in fallout Pu from the PPG was more efficiently scavenged from surface water than Pu derived from global fallout. We thus contend that scavenging of PPG-sourced Pu from surface water and its ultimate deposition into the sediment are the plausible cause for the observed decline in the PPG Pu-fraction. It must be pointed out that the difference in the PPG Pu-fraction in the IPI during the past 20 years is not large and within the range of spatial variation, suggesting that the net effect of Pu scavenging on the PPG Pu-fraction in the IPI is relatively small.

The fractional contribution of PPG close-in fallout Pu in the IS is  $34 \pm 8\%$ , which lies between the mean fraction in the WP ( $17 \pm 5\%$ ) and that in the SCS ( $49 \pm 3\%$ ) (Fig. 6). The mean PPG Pu-fraction at the ITF entrance ( $27 \pm 2\%$ ) is lower than that within the IS ( $36 \pm 3\%$ ), and the highest PPG Pu-fractions are observed at the ITF exit ( $45 \pm 3\%$ ) in the IS. The distribution pattern further indicates that the SCS, as the water source with the higher PPG Pu-fraction, is transported into the IS and mixed with the water mass from the WP.

#### 4.3. Water mass fraction from the South China Sea in the Indonesian seas

As the secondary ITF water source, the water mass from the SCS, is transported into the IS via the Karimata and Mindoro Straits (Gordon et al., 2012; Qu et al., 2006). The PPG derived Pu-fraction is calculated from the Pu atom ratio using Eq. (1), which is a conservative signal. The relationship between the PPG derived Pu-fraction and salinity (traditional conservative parameter) in the IS represents a two-endmember mixing scheme between the SCS and WP waters (Fig. 7). All the data in the interior IS fall into the conservative mixing region (gray shadow), again indicating that the PPG derived Pu-fraction can be regarded as being conservative in our uncertainty calculation. Because the water masses at the ITF exit are affected by the water exchange with the Indian

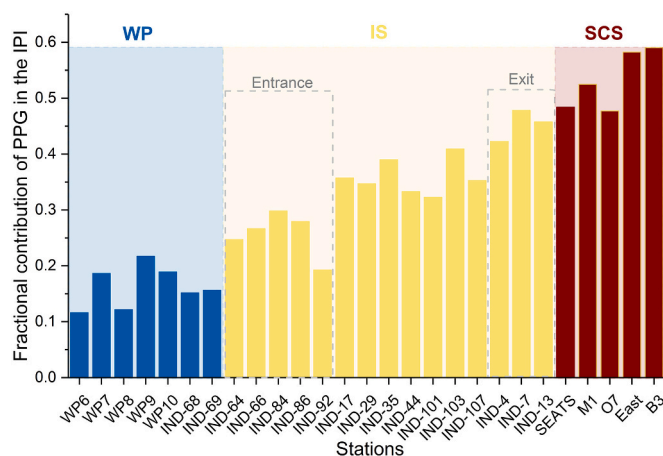


Fig. 6. Fractional contribution of Pu from the Pacific Proving Grounds in surface water at various stations in the Indo-Pacific Intersection. WP, IS and SCS denote the samples from different Western Pacific Ocean, Indonesian Seas and South China Sea stations, respectively. The two gray dashed boxes indicate the stations at the entrance and exit of main ITF pathway.

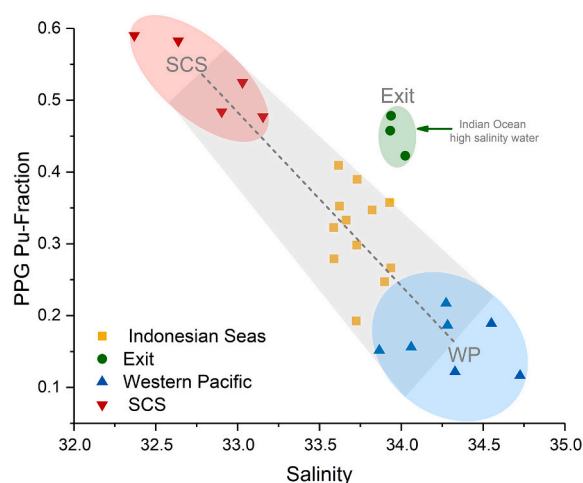


Fig. 7. Fractional contribution of Plutonium (Pu) derived from the Pacific Proving Grounds (PPG) vs. salinity in surface water of the Indo-Pacific Intersection. Red triangles, blue triangles and yellow squares indicate samples collected from the Western Pacific Ocean (WP), South China Sea (SCS) and Indonesian Seas (IS), respectively. Green circles indicate samples collected from the Ombai Strait and Timor Passage at the Indonesian Throughflow (ITF) exit. (For interpretation of the references to colour in this figure legend, the reader is referred to the web version of this article.)

Ocean water of high salinity, they shift away from the two-endmember mixing scheme and exhibit higher salinities.

The residence time of the water mass in the IS is only 2.5 years for upper 250 m water column (Xie et al., 2019). Almost all of the early deposition of close-in fallout Pu had been transported into the Indian Ocean with very limited residuals remained in the IS. Therefore, the Pu-PPG in the IS is controlled by the Pu transported from the SCS and WP. To estimate the water mass fraction from the SCS in IS surface water, a two-endmember mixing model based on PPG derived Pu contribution was used as follows:

$$f_{SCS} \cdot C_{SCS} \cdot F_{SCS} + (1 - f_{SCS}) \cdot C_{WP} \cdot F_{WP} = C_{IS} \cdot F_{IS} \quad (2)$$

where,  $F_{SCS}$  and  $F_{WP}$  are the average fractional contributions of Pu derived from PPG for SCS and WP endmembers, respectively;  $C_{SCS}$  and  $C_{WP}$  are the average values of Pu activity for SCS and WP endmembers, respectively;  $C_{IS}$  and  $F_{IS}$  are the Pu activities and PPG derived Pu-fractions in the IS;  $f_{SCS}$  is the water mass fraction transported from the SCS in the IS;  $f_{SCS} \cdot C_{SCS} \cdot F_{SCS}$  represents the PPG-derived Pu transported from the SCS;  $(1 - f_{SCS}) \cdot C_{WP} \cdot F_{WP}$  represents the PPG-derived Pu transported from the WP;  $C_{IS} \cdot F_{IS}$  represents the PPG-derived Pu in the IS.

The average fraction of the SCS water mass in surface IS is estimated to be  $35 \pm 16\%$ . Based on 3 year-mooring observations from the INSTANT project, the total ITF transport in the upper 235 m is about 10 Sv (Sprintall et al., 2009). Results of the numerical model reveal that the total  $4.3 \pm 1.2$  Sv water mass outflow from the SCS into the IS contributes  $\sim 43\%$  of the ITF transport (Gan et al., 2016). Our estimate agrees well with that derived from physical measurements.

Sibutu passage is the main channel for the transport of SCS water mass into the IS (Gordon et al., 2012; Liu and Gan, 2017; Sprintall et al., 2012). Thus, the fraction of SCS water at Makassar Strait is higher at  $59\% \pm 18\%$  than the average fraction (Fig. 8). The IS entrance shows the lowest SCS water mass fraction with an average value of  $5\% \pm 8\%$ , implying the SCS water mass is mainly transported southward after entering the Sulawesi Sea. The Karimata Strait is the second channel available for exiting of the water mass from the SCS into the IS. The latter will merge into the water mass transported from the ITF main pathway (Makassar Strait) and partly heads to the eastern IS (Fang et al., 2010; He et al., 2015). Based on the PPG Pu contribution, it can be

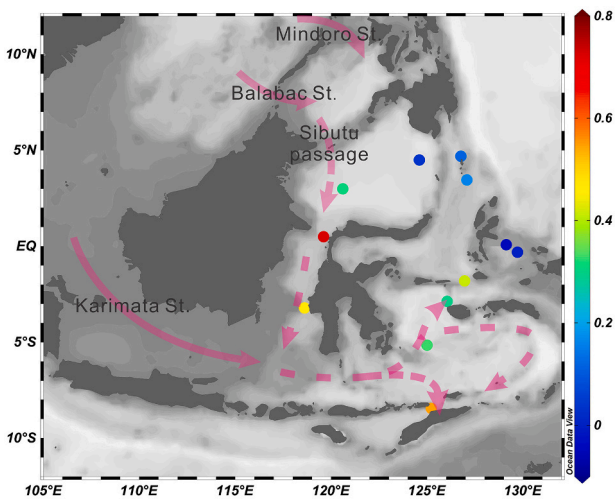


**Fig. 8.** Fractional contributions of SCS water mass through the various straits to surface water of the Indonesian Seas shown using colored dots. Solid and dashed pink lines indicate the transport pathway of SCS water mass at the straits exiting SCS and within the Indonesian Seas. Colour bar indicates the ratio of SCS water mass to total water mass. (For interpretation of the references to colour in this figure legend, the reader is referred to the web version of this article.)

estimated that the SCS contributes  $34\% \pm 6\%$  of surface water to the Banda Sea and Lifamatola Strait.

Depth of the topographic sill connecting the SCS/Sulu Seas and IS is  $\sim 235$  m at the Sibutu passage (Gordon et al., 2012). It is here assumed that buoyant freshwater from local river discharge and precipitation mainly resides in the upper layer and that its influence on the water below the mixed layer ( $\sim 50$  m depth) is limited; therefore the two-endmember mixing model based on salinity was used to estimate the SCS water mass fraction between 50 m and 235 m (Du et al., 2013), as follows:

$$f_{SCS} \cdot S_{SCS} + (1 - f_{SCS}) \cdot S_{WP} = S_{IND} \quad (5)$$

where the SCS water fraction is denoted as  $f_{SCS}$ ,  $1 - f_{SCS}$  is the WP water fraction, and  $S_{WP}$  and  $S_{SCS}$  denote the salinities of the Pacific and SCS endmembers at the corresponding density. The observed salinity in the IS is indicated as  $S_{IND}$ , and the PR24 section (World Ocean Circulation Experiment, WOCE) across the ITF gateway region, which was also sampled in October, is taken to represent the WP endmember.

Observations based on CTD data revealed that the upper thermocline profile down to an isopycnal of potential density ( $\sigma_\theta = 25.8$ ) ( $< 200$  m) was strongly influenced by vertical mixing, with isopycnal mixing becoming dominant in the lower thermocline (Gordon, 2005; Hautala et al., 1996). Thus, we will not discuss the estimated SCS fraction for each observed water parcel between 50 m and 235 m. Instead, the water column integrated values of the estimated SCS water mass fractions over this depth range are used for the following SCS freshwater fractional estimation. The average fractional contribution of SCS water between 50 m and 235 m in the IS is estimated to be  $49 \pm 14\%$ , which is comparable to the  $\sim 43\%$  mean contribution of the SCSTF to the ITF obtained by numerical modeling (SCSTF:  $4.3 \pm 2.78$  Sv; Gan et al., 2016) and 3 years time-series observations (ITF: 10 Sv; Sprintall et al., 2009). The high-resolution ( $0.1^\circ \times 0.1^\circ$ ) regional ocean model, however, showed strong opposite interannual variability of the ITF and SCSTF associated with the ENSO, with Sibutu flow increasing on average by 1.2 Sv and Mindanao–Sulawesi flow declining by 2.4 Sv in El Niño years (Wei et al., 2016). As a result, our estimate is substantially higher than the fractional contribution of SCS water derived from limited field observations of SCSTF transport in the Karimata Strait ( $0.5 \pm 1.9$  Sv) and Mindoro Strait (0.1 Sv) in 2008, which coincided with a strong La Niña event when the

Pacific inflow into the SCS is expected to be weaker, and subsequent transports are lower (Susanto et al., 2013; Sprintall et al., 2012). Thus, considering the obvious seasonal and inter-annual variability of the SCSTF, our tracer-based approach provides a temporally integrated value, which is advantageous over short-term field observations.

#### 4.4. Freshwater flux from the South China Sea to the Indian Ocean

The buoyant upper water associated with the SCSTF, typically characterized by lower salinity than that in the WP, is transported into the IS via the Sibutu Passage and Karimata Strait. Based on the estimated fractions of SCS water mass, the freshwater fractions from the SCS can be calculated as follows:

$$F_{fw} = \frac{S_0 - S_{SCS}}{S_0} \cdot f_{SCS} \quad (3)$$

where  $F_{fw}$  is the fraction of freshwater from the SCS in the IS;  $f_{SCS}$  is the fraction of water mass transported into the IS from the SCS;  $S_{SCS}$  is the salinity of the SCS endmember and  $S_0$  is the reference salinity. The freshwater fraction in the SCS is defined as  $f_{fw} = \frac{S_0 - S_{SCS}}{S_0}$ . The climatologically mean salinity of 34.62 at the similar meridional section from the southern Tasmania to  $50^\circ$ S is selected to be the reference salinity as previously did in the literature (Fang et al., 2010; Susanto et al., 2013), which is the original water source of the Pacific water transported from the south Indian Ocean (Levitus and Boyer, 1994).

For surface water, the highest freshwater fraction from the SCS at  $3.1 \pm 0.9\%$  is observed in the Makassar Strait. The fractions of SCS freshwater in the Sulawesi Sea exhibit spatial variation: they are lower in the northern Sulawesi Sea ranging between 0.2% and 0.8%. In the southern Sulawesi Sea, the fraction is higher at 1.6%, implying that the Sibutu passage is also an important channel to transport the buoyant SCS water mass to the IS, while  $\sim 2.0 \pm 0.7\%$  freshwater from the SCS is transported to the Banda Sea.

Taking the volume of each region as the weight, the spatially averaged freshwater fraction from the SCS in the IS is estimated as follows:

$$\bar{F}_{fw\_SCS} = \frac{\sum (V_i \cdot F_{fwi})}{\sum V_i} \quad (4)$$

where  $V_i$  is the volume of each region,  $F_{fwi}$  is the mean freshwater fraction from the SCS in the corresponding region, and  $\bar{F}_{fw\_SCS}$  is the average freshwater fraction from the SCS in the IS.

The average freshwater fraction from the SCS is estimated at  $1.7 \pm 0.3\%$  in the IS mixed layer ( $\sim 50$  m), corresponding to  $1.7 \times 10^{12}$  km<sup>3</sup> SCS freshwater. The long-term moorings deployed in the IS showed that the mean ITF water mass transport was 2.7 Sv for the upper 50 m (Sprintall et al., 2009). It is estimated that a mean freshwater flux of  $\sim 46$  mSv is transported from the SCS to the Indian Ocean in the upper 50 m. Comparing with the mixed layer, the average freshwater fraction from the SCS between 50 m and 235 m is much smaller in the IS, averaging  $0.5 \pm 0.1\%$ . If we integrate the upper 235 m water column, the average freshwater fraction from the SCS in the IS is  $0.8 \pm 0.4\%$ .

The water mass flux that exits the IS into the Indian Ocean is  $\sim 10$  Sv in the upper  $\sim 235$  m based on both physical and chemical tracer observations, contributing  $\sim 25\%$  in the upper 50 m and  $\sim 75\%$  between 50 m and 235 m (Sprintall et al., 2009; Xie et al., 2019). The mean transport-weighted freshwater flux from the SCS into the Indian Ocean is estimated at  $80 \pm 47$  mSv. Since the annual mean transport-weighted salinity is 34.6 in the Luzon Strait, similar to our reference salinity (Qu et al., 2006), freshwater transport through the Luzon Strait is considered negligible. Based on numerical modeling, the freshwater budgets of the SCS revealed that the net freshwater flux through the Luzon and Taiwan Straits was only  $-16$  mSv (Fang et al., 2009). Thus, the  $80 \pm 47$  mSv freshwater transported from the SCS to the IS is derived from P-E over the SCS and the land discharge surrounding the SCS. The average water mass transit time in the IS is  $\sim 2$  years in the upper 250 m

(Xie et al., 2019), which suggests that estimates derived in the present study from the chemical tracer reflect an integrated result on an inter-annual timescale. The salinity of the SCS endmember has a spatial variation from 32.37 to 33.15 with an average value of  $32.82 \pm 0.32$ . Based on Eq. (3), this variation will translate into an uncertainty of 17% ( $\frac{\text{Uncertainty}_{\text{SCS}}}{(S_0 - S_{\text{SCS}})} = \frac{0.32}{(34.62 - 32.82)}$ ), which corresponds to about 13.6 mSv in volume transport. Besides, due to the seasonal variation, the mean salinity in the eastern SCS ranges from 32.49 to 32.98 in the upper 50 m and remains relatively consistent seasonally ( $34.37 \pm 0.02$ ) between 50 m and 250 m (WOD: World Ocean Database). If the maximum seasonal salinity variation is used to assess the potential uncertainty, and the salinities in one season are taken to represent the SCS endmember value, at most  $\sim 7$  mSv uncertainty can be associated with our results.

Field observations conducted in the Mindoro and Balabac Straits are much fewer than those available from the Karimata Strait. Nevertheless, the pronounced seasonal and interannual variability in the Karimata Strait compound the observed results. Thus, available accurate estimates of freshwater transport associated with the SCSTF are limited. Moorings deployed in the Karimata Strait yielded a freshwater flux in the boreal winter month of 140 mSv (Fang et al., 2010). In boreal summer, the transport through the Karimata Strait reverses with  $-120$  mSv freshwater, suggesting that the annual mean will be much smaller than seasonal results (Susanto et al., 2013). Observations spanning 10 years in the Karimata Strait showed that the annual mean volume transport is  $\sim 0.75$  Sv (Wei et al., 2019). If the observed long-term water mass flux and the mean salinity of the upper 50 m water column (32.93, WOD,  $n = 2731$ ) south of  $3^\circ\text{N}$  SCS are used to roughly estimate freshwater transport, the calculations yield a freshwater flux of 37 mSv for the Karimata Strait. The long-term direct measurements of currents and salinity in the Karimata Strait indicate an annual mean freshwater transport of  $30.87 \pm 6.15$  mSv (Xu et al., 2021), which is consistent to the present estimate. The 35 mSv freshwater is transported through the Mindoro and Balabac Straits as derived from the model (Fang et al., 2009). Taken together, a total of 72 mSv freshwater transport is suggested to flow from the SCS to the IS, comparable to our results.

Qu et al. (2006) used the high-resolution Ocean General Circulation Model (OGCM) for the Earth Simulator (OFES) and World Ocean Atlas 1998 (WOA98) salinity data to estimate that 40 mSv freshwater from the SCS was transported into the IMC, if we convert their adopted reference salinity (35) into that used in the present study. It is noteworthy that river runoff is not included in Qu et al.'s (2006) model because data are not readily available. Consequently, these authors estimated a lower flux than that obtained in the present study. Based on the model (MOM2)-derived SCS freshwater budgets, Fang et al. (2009) estimated a total annual land discharge to the SCS and annual  $P - E$  over the SCS of  $1.60 \times 10^{12}$  and  $1.94 \times 10^{12} \text{ m}^3 \text{ year}^{-1}$ , respectively, which indicates that the SCS contribution of freshwater to the IS is 87 mSv. All these prior independent estimates are comparable to that derived in the present study.

Based on the global freshwater budget, Talley et al. (2008) estimated that the freshwater flux from the ITF into the Indian Ocean was  $230 \pm 50$  mSv. If we convert these authors' adopted reference salinity (34.9) into that used in the present study (34.62), a value similar to the average salinity of the WP upper 235 m water at the gateway region (34.64), it is calculated that  $150 \pm 32$  mSv freshwater is transported into the Indian Ocean by the ITF, indicating that the SCS contributes  $53 \pm 31\%$  of the total ITF freshwater flux. The precipitated water over the land of Indonesia will partly enter the IS via river discharge, adding to about 10 mSv (Kida et al., 2019). The freshwater flux from the SCS is 8 times higher than the local river discharge. The integrated precipitation ( $P$ ) and evaporation ( $E$ ) over the IS determined from the Ocean General Circulation Model for the Earth Simulator (OFES2) is 60 mSv, accounting for  $\sim 40\%$  ITF freshwater flux (Kida et al., 2019; Talley, 2008). Our estimate for the SCS freshwater flux into the IS balances well with the total ITF freshwater,  $P-E$  flux and river discharge in the IS derived from independent research.

The hydrological cycle in the Indian Ocean yields a net evaporation of 340 mSv based on mean surface fluxes integrated over  $8^\circ\text{N}$  to  $32^\circ\text{S}$  of the Indian Ocean (Talley, 2008). The quantified relative contribution of the SCS to the IS freshwater reveals that the SCSTF supplies  $\sim 24\%$  freshwater loss for air-sea exchange in the Indian Ocean. The evaporated freshwater from the Indian Ocean will mainly be transported eastward under the effect of the monsoon via atmospheric circulation, and then partly fall out in marginal seas and the maritime continent (Yamanaka et al., 2018). The SCS receives substantial freshwater associated with the Asian monsoon via river discharge and precipitation, which is found to be mostly transported back to the Indian Ocean. Therefore, although the SCSTF is highly variable, the temporally integrated SCS freshwater flux into the Indian Ocean indicates that the SCS, together with the SCS branch of the Pacific-Indian Oceans Throughflow, play a critical role in maintaining the freshwater balance in both the IPI and Indian Ocean.

Furthermore, the fresher SCS upper layer water transported into the IS is able to reduce the mean density of the upper 235 m water layer to  $\sim 0.2 \text{ kg m}^{-3}$ , an amount sufficient to decrease the southward pressure gradient and inhibit the transport of upper layer water at higher temperature from the western tropical Pacific warm pool into the Indian Ocean. As a feedback, the cooler Indian Ocean sea surface temperature due to the SCS freshwater transport will in turn weaken the surface air-sea flux and the SCS freshwater input (Gordon et al., 2003; Yamanaka et al., 2018). Thus, the fresher SCS and its throughflow, analogous to an 'air conditioner', also plays a critical role in regulating the IPI and Indian Ocean heat balance.

## 5. Conclusions

Analysis of the Pu isotopic composition ( $^{240}\text{Pu}/^{239}\text{Pu}$ : 0.194–0.258) indicates that Pu in the IPI is sourced from both global and PPG close-in fallout. A freshwater influx of  $80 \pm 47$  mSv was quantified from the SCS to the IS, a load that decreases the mean density of the upper 235 m by  $\sim 0.2 \text{ kg m}^{-3}$ . This density change and the subsequent decrease in the southward pressure gradient in the IS are able to regulate the water mass and heat transport from the western tropical Pacific warm pool into the Indian Ocean. The integrated SCS freshwater flux into the IS is equivalent to over half ( $53 \pm 31\%$ ) the total freshwater flux transported by the ITF into the Indian Ocean and can supply  $\sim 24\%$  the freshwater net evaporation in the Indian Ocean over the  $8^\circ\text{N}$  to  $32^\circ\text{S}$  latitudinal range, demonstrating that the SCSTF provides an important linkage of the atmosphere-ocean water cycle between the IPI and the Indian Ocean. In conclusion, both the heat and freshwater balance in the IPI and Indian Ocean are strongly regulated by the SCS and its throughflow.

## Declaration of Competing Interest

The authors declare that they have no known competing interests.

## Acknowledgements

This study was supported by National Natural Science Foundation of China through grants No. 41890804, 41730533 and the "Strategic Priority Research Program" of the Chinese Academy of Sciences through grants No. XDB42000000. The authors thank the captains and crew of the R/V Dongfanghong II and R/V Baruna Jaya VIII for their assistance in sampling during the cruise, and Yaojin Chen for providing assistance in sample analysis.

## References

- Bu, W., Fukuda, M., Zheng, J., Aono, T., Ishimaru, T., Kanda, J., Yang, G., Tagami, K., Uchida, S., Guo, Q., 2014a. Release of Pu isotopes from the Fukushima Daiichi Nuclear Power Plant accident to the marine environment was negligible. *Environ. Sci. Technol.* 48 (16), 9070–9078.
- Bu, W., Zheng, J., Guo, Q., Aono, T., Tagami, K., Uchida, S., Tazoe, H., Yamada, M., 2014b. Ultra-trace plutonium determination in small volume seawater by sector field

- inductively coupled plasma mass spectrometry with application to Fukushima seawater samples. *J. Chromatogr. A* 1337, 171–178.
- Bu, W., Zheng, J., Guo, Q., Aono, T., Tazoe, H., Tagami, K., Uchida, S., Yamada, M., 2014c. A method of measurement of  $^{239}\text{Pu}$ ,  $^{240}\text{Pu}$ ,  $^{241}\text{Pu}$  in high U content marine sediments by sector field ICP-MS and its application to Fukushima sediment samples. *Environ. Sci. Technol.* 48 (1), 534–541.
- Buesseler, K.O., 1997. The isotopic signature of fallout plutonium in the North Pacific. *J. Environ. Radioact.* 36 (1), 69–83.
- Buesseler, K.O., Halverson, J.E., 1987. The mass spectrometric determination of fallout  $^{239}\text{Pu}$  and  $^{240}\text{Pu}$  in marine samples. *J. Environ. Radioact.* 5 (6), 425–444.
- Buesseler, K.O., Charette, M.A., Pike, S.M., Henderson, P.B., Kipp, L.E., 2018. Lingering radioactivity at the Bikini and Eniwetok Atolls. *Sci. Total Environ.* 621, 1185–1198.
- Choppin, G.R., 2006. Actinide speciation in aquatic systems. *Mar. Chem.* 99 (1), 83–92. <https://doi.org/10.1016/j.marchem.2005.03.011>.
- Dai, M., Buesseler, K.O., Pike, S.M., 2005. Plutonium in groundwater at the 100K-Area of the U.S. DOE Hanford Site. *J. Contam. Hydrol.* 76 (3), 167–189. <https://doi.org/10.1016/j.jconhyd.2004.08.004>.
- Du, C., Liu, Z., Dai, M., Kao, S.-J., Cao, Z., Zhang, Y., Huang, T., Wang, L., Li, Y., 2013. Impact of the Kuroshio intrusion on the nutrient inventory in the upper northern South China Sea: insights from an isopycnal mixing model. *Biogeosciences* 10 (10), 6419–6432.
- Fang, G., Wang, Y., Wei, Z., Fang, Y., Qiao, F., Hu, X., 2009. Inter-ocean circulation and heat and freshwater budgets of the South China Sea based on a numerical model. *Dyn. Atmos. Oceans* 47 (1–3), 55–72.
- Fang, G., Susanto, R.D., Wirasantosa, S., Qiao, F., Supangat, A., Fan, B., Wei, Z., Sulistiyo, B., Li, S., 2010. Volume, heat, and freshwater transports from the South China Sea to Indonesian seas in the boreal winter of 2007–2008. *J. Geophys. Res. Oceans* (1978–2012) 115 (C12).
- Gan, J., Liu, Z., Liang, L., 2016. Numerical modeling of intrinsically and extrinsically forced seasonal circulation in the China Seas: a kinematic study. *J. Geophys. Res. Oceans* 121 (7), 4697–4715.
- Gordon, A.L., 1986. Inter-ocean exchange of thermocline water. *J. Geophys. Res. Oceans* 91 (C4), 5037–5046. <https://doi.org/10.1029/JC091iC04p05037>.
- Gordon, A.L., 2005. Oceanography of the Indonesian Seas and their throughflow. *Oceanography* 18 (4), 14.
- Gordon, A.L., Susanto, R.D., Vranes, K., 2003. Cool Indonesian throughflow as a consequence of restricted surface layer flow. *Nature* 425 (6960), 824–828.
- Gordon, A.L., Huber, B.A., Metzger, E.J., Susanto, R.D., Hurlburt, H.E., Adi, T.R., 2012. South China Sea throughflow impact on the Indonesian throughflow. *Geophys. Res. Lett.* 39 (11).
- Guohong, F., Susanto, D., Soesilo, I., Zheng, Q.A., Fangli, Q., Zexun, W., 2005. A note on the South China Sea shallow inter-ocean circulation. *Adv. Atmos. Sci.* 22 (6), 946–954. <https://doi.org/10.1007/BF02918693>.
- Gutknecht, E., Refrayr, G., Gehlen, M., Triyulianti, I., Berlianty, D., Gaspar, P., 2016. Evaluation of an operational ocean model configuration at  $1/12^\circ$  spatial resolution for the Indonesian seas (NEMO2.3/INDO12) - Part 2: Biogeochemistry. *Geosci. Model Dev.* 9 (4), 1523–1543. <https://doi.org/10.5194/gmd-9-1523-2016>.
- Hautala, S.L., Reid, J.L., Bray, N., 1996. The distribution and mixing of Pacific water masses in the Indonesian Seas. *J. Geophys. Res.* 101 (C5), 12375–12389. <https://doi.org/10.1029/96jc00037>.
- He, Z., Feng, M., Wang, D., Slawinski, D., 2015. Contribution of the Karimata Strait transport to the Indonesian Throughflow as seen from a data assimilation model. *Cont. Shelf Res.* 92, 16–22.
- Hirose, K., Aoyama, M., Kim, C.S., 2007. Plutonium in seawater of the Pacific Ocean. *J. Radioanal. Nucl. Chem.* 274 (3), 635–638. <https://doi.org/10.1007/s10967-006-6946-5>.
- Kelley, J.M., Bond, L.A., Beasley, T.M., 1999. Global distribution of Pu isotopes and  $^{237}\text{Np}$ . *Sci. Total Environ.* 237 (238), 483–500. [https://doi.org/10.1016/S0048-9697\(99\)00160-6](https://doi.org/10.1016/S0048-9697(99)00160-6).
- Kershaw, P., Woodhead, D., Lovett, M., Leonard, K., 1995. Plutonium from European reprocessing operations—its behaviour in the marine environment. *Appl. Radiat. Isot.* 46 (11), 1121–1134.
- Kida, S., Richards, K.J., Sasaki, H., 2019. The fate of surface freshwater entering the Indonesian Seas. *J. Geophys. Res. Oceans* 124 (5), 3228–3245. <https://doi.org/10.1029/2018jc014707>.
- Krey, P., Hardy, E., Pachucki, C., Rourke, F., Coluzza, J., Benson, W., 1975. Mass isotopic composition of global fallout plutonium in soil. In: *Transuranium Nuclides in the Environment*, 671–678.
- Levitus, S., Boyer, T., 1994. *World Ocean Atlas*. National Oceanic & Atmospheric Administration, Washington, D. C. p. 117.
- Li, M., Wei, J., Wang, D., Gordon, A.L., Yang, S., Malanotte-Rizzoli, P., Jiang, G., 2019. Exploring the importance of the Mindoro-Sibutu pathway to the upper-layer circulation of the South China Sea and the Indonesian throughflow. *J. Geophys. Res. Oceans* 124 (7), 5054–5066. <https://doi.org/10.1029/2018jc014910>.
- Liu, Z., Gan, J., 2017. Three-dimensional pathways of water masses in the South China Sea: a modeling study. *J. Geophys. Res. Oceans* 122 (7), 6039–6054.
- Lukas, R., Firing, E., Hacker, P., Richardson, P.L., Collins, C.A., Fine, R., Gammon, R., 1991. Observations of the Mindanao current during the western equatorial Pacific Ocean circulation study. *J. Geophys. Res.* 96 (C4), 7089–7104. <https://doi.org/10.1029/91jc00062>.
- Mocak, J., Bond, A.M., Mitchell, S., Scollary, G., 1997. A statistical overview of standard (IUPAC and ACS) and new procedures for determining the limits of detection and quantification: application to voltammetric and stripping techniques (technical report). *Pure Appl. Chem.* 69 (2), 297–328.
- Morey, S.L., Shriver, J.F., O'Brien, J.J., 1999. The effects of Halmahera on the Indonesian throughflow. *J. Geophys. Res.* 104 (C10), 23281–23296.
- Muramatsu, Y., Hamilton, T., Uchida, S., Tagami, K., Yoshida, S., Robison, W., 2001. Measurement of  $^{240}\text{Pu}/^{239}\text{Pu}$  isotopic ratios in soils from the Marshall Islands using ICP-MS. *Sci. Total Environ.* 278 (1), 151–159.
- Pham, M., Betti, M., Povinec, P., Benmansour, M., Bünger, V., Drefvelin, J., Engeler, C., Flemal, J., Gascó, C., Guillevic, J., 2011. A certified reference material for radionuclides in the water sample from Irish Sea (IAEA-443). *J. Radioanal. Nucl. Chem.* 288 (2), 603–611.
- Pittauer, D., Tims, S.G., Froehlich, M.B., Fifield, L.K., Wallner, A., McNeil, S.D., Fischer, H.W., 2017. Continuous transport of Pacific-derived anthropogenic radionuclides towards the Indian Ocean. *Sci. Rep.* 7 (44679) <https://doi.org/10.1038/srep44679>.
- Qu, T., Du, Y., Sasaki, H., 2006. South China Sea throughflow: a heat and freshwater conveyor. *Geophys. Res. Lett.* 33 (23).
- Sholkovitz, E.R., 1983. The geochemistry of plutonium in fresh and marine water environments. *Earth Sci. Rev.* 19 (2), 95–161.
- Sprintall, J., Wijffels, S.E., Molcard, R., Jaya, I., 2009. Direct estimates of the Indonesian Throughflow entering the Indian Ocean: 2004–2006. *J. Geophys. Res. Oceans* 114 (C07001). <https://doi.org/10.1029/2008JC005257>.
- Sprintall, J., Gordon, A.L., Flament, P., Villanoy, C.L., 2012. Observations of exchange between the South China Sea and the Sulu Sea. *J. Geophys. Res. Oceans* (1978–2012) 117 (C5).
- Sprintall, J., Gordon, A.L., Koch-Larrouy, A., Lee, T., Potemra, J.T., Pujiana, K., Wijffels, S.E., 2014. The Indonesian seas and their role in the coupled ocean-climate system. *Nat. Geosci.* 7, 487–492. <https://doi.org/10.1038/NNGEO2188>.
- Susanto, R.D., Wei, Z., Adi, R.T., Fan, B., Li, S., Fang, G., 2013. Observations of the Karimata Strait throughflow from December 2007 to November 2008. *Acta Oceanol. Sin.* 32 (5), 1–6. <https://doi.org/10.1007/s13131-013-0307-3>.
- Talley, L.D., 2008. Freshwater transport estimates and the global overturning circulation: Shallow, deep and throughflow components. *Prog. Oceanogr.* 78 (4), 257–303. <https://doi.org/10.1016/j.poccean.2008.05.001>.
- Tozuka, T., Qu, T., Masumoto, Y., Yamagata, T., 2009. Impacts of the South China Sea Throughflow on seasonal and interannual variations of the Indonesian Throughflow. *Dyn. Atmos. Oceans* 47 (1), 73–85. <https://doi.org/10.1016/j.dynatmoce.2008.09.001>.
- Wang, Y., Xu, T., Li, S., Susanto, R.D., Agustiani, T., Trenggono, M., Tan, W., Wei, Z., 2019. Seasonal variation of water transport through the Karimata Strait. *Acta Oceanol. Sin.* 38 (4), 47–57. <https://doi.org/10.1007/s13131-018-1224-2>.
- Wei, J., Li, M., Malanotte-Rizzoli, P., Gordon, A.L., Wang, D.X., 2016. Opposite variability of Indonesian throughflow and South China Sea throughflow in the Sulawesi Sea. *J. Phys. Oceanogr.* 46 (10), 3165–3180. <https://doi.org/10.1175/JPO-D-16-0132.1>.
- Wei, Z., Li, S., Susanto, R.D., Wang, Y., Fan, B., Xu, T., Sulistiyo, B., Adi, T.R., Setiawan, A., Kuswardani, A., Fang, G., 2019. An overview of 10-year observation of the South China Sea branch of the Pacific to Indian Ocean throughflow at the Karimata Strait. *Acta Oceanol. Sin.* 38 (4), 1–11. <https://doi.org/10.1007/s13131-019-1410-x>.
- Wu, J., Zheng, J., Dai, M., Huh, C.-A., Chen, W., Tagami, K., Uchida, S., 2014. Isotopic composition and distribution of Plutonium in northern South China Sea sediments revealed continuous release and transport of Pu from the Marshall Islands. *Environ. Sci. Technol.* 48 (6), 3136–3144.
- Wu, J., Dai, M., Xu, Y., Zheng, J., 2018. Sources and accumulation of plutonium in a large Western Pacific marginal sea: the South China Sea. *Sci. Total Environ.* 610, 200–211.
- Wu, J., Dai, M., Xu, Y., Zheng, J., 2019. Plutonium in the western North Pacific: Transport along the Kuroshio and implication for the impact of Fukushima Daiichi Nuclear Power Plant accident. *Chem. Geol.* 511, 256–264. <https://doi.org/10.1016/j.chemgeo.2018.12.006>.
- Xie, T., Newton, R., Schlosser, P., Du, C., Dai, M., 2019. Long-term mean mass, heat and nutrient flux through the Indonesian Seas, based on the Tritium inventory in the Pacific and Indian Oceans. *J. Geophys. Res. Oceans* 124 (6), 3859–3875. <https://doi.org/10.1029/2018jc014863>.
- Xu, T., Wei, Z., Susanto, R.D., Li, S., Wang, Y., Wang, Y., et al., 2021. Observed water exchange between the South China Sea and Java Sea through Karimata Strait. *J. Geophys. Res. Oceans* 126, e2020JC016608. <https://doi.org/10.1029/2020JC016608>.
- Yamada, M., Zheng, J., Wang, Z.-L., 2006.  $^{137}\text{Cs}$ ,  $^{239+240}\text{Pu}$  and  $^{240}\text{Pu}/^{239}\text{Pu}$  atom ratios in the surface waters of the western North Pacific Ocean, eastern Indian Ocean and their adjacent seas. *Sci. Total Environ.* 366 (1), 242–252.
- Yamanaka, M.D., Ogino, S.-Y., Wu, P.-M., Jun-Ichi, H., Mori, S., Matsumoto, J., Syamsudin, F., 2018. Maritime continent coastlines controlling Earth's climate. *Prog. Earth Planet. Sci.* 5 (1), 21. <https://doi.org/10.1186/s40645-018-0174-9>.
- Yaremchuk, M., McCreary Jr., J., Yu, Z., Furue, R., 2009. The South China Sea throughflow retrieved from climatological data. *J. Phys. Oceanogr.* 39 (3), 753–767. <https://doi.org/10.1175/2008JPO3955.1>.
- Zheng, J., Yamada, M., 2007. Precise determination of Pu isotopes in a seawater reference material using ID-SF-ICP-MS combined with two-stage anion-exchange chromatography. *Anal. Sci.* 23 (5), 611–615.
- Zheng, J., Aono, T., Uchida, S., Zhang, J., Honda, M.C., 2012. Distribution of Pu isotopes in marine sediments in the Pacific 30 km off Fukushima after the Fukushima Daiichi nuclear power plant accident. *Geochem. J.* 46 (4), 361–369.